

# Non-local Plasma Spectrum of Graphene interacting with a Thick Conductor

Godfrey Gumbs<sup>1,2</sup>, Andrii Iurov<sup>1,4</sup>, and N. J. M. Horing<sup>3</sup>

<sup>1</sup>*Department of Physics and Astronomy, Hunter College of the City University of New York, 695 Park Avenue, New York, NY 10065, USA*

<sup>2</sup>*Donostia International Physics Center (DIPC), P de Manuel Lardizabal, 4, 20018 San Sebastian, Basque Country, Spain*

<sup>3</sup>*Department of Physics and Engineering Physics,*

*Stevens Institute of Technology, Hoboken, NJ 07038, USA*

<sup>4</sup>*Center for High Technology Materials, University of New Mexico, NM 87106, USA*

(Dated: November 1, 2021)

Self-consistent field theory is used to obtain the non-local plasmon dispersion relation of monolayer graphene which is Coulomb-coupled to a thick conductor. We calculate numerically the undamped plasmon excitation spectrum for arbitrary wave number. For gapped graphene, both the low-frequency (acoustic) and high frequency (surface) plasmons may lie within an undamped opening in the particle-hole region. Furthermore, we obtain plasmon excitations in a region of frequency-wave vector space which do not exist for free-standing gapped graphene.

PACS numbers: 73.21.-b, 71.70.Ej, 73.20.Mf, 71.45.Gm, 71.10.Ca, 81.05.ue

## I. INTRODUCTION

Recent research on plasmon excitations<sup>1-4</sup> has covered fundamental aspects such as nonlocality<sup>5</sup>, quantum effects in nanoscale structures including fullerene<sup>6-8</sup>, graphene<sup>9,10</sup>, carbon nanotubes<sup>11,12</sup>, silicene<sup>13,14</sup> and metallic dimers<sup>15</sup>, surface plasmon lasing<sup>16</sup>, plasmon-electron interaction<sup>17</sup> and the potential role played by plasmon excitations in electronic sensors<sup>18,19</sup> and radiation degradation of electronic and optoelectronic devices<sup>20</sup>. The surge in activity to understand and discover novel plasmonic materials is stimulated by possible applications such as light concentration for solar energy<sup>21</sup>, devices for telecommunications<sup>22</sup>, and near-field instrumentation<sup>23</sup>. Investigation of the damped terahertz plasmons in graphene, interacting with surface plasmons of a substrate with a large doping due to a large scattering rate, was addressed in<sup>24</sup>. The authors demonstrated that the field spread of the graphene plasmons into the substrate suppressed.

In view of the stated importance of achieving a detailed understanding of plasma excitations, we devote this paper to a specific area which has not been adequately covered so far in the literature. It concerns plasmon excitations in monolayer graphene. There are several papers dealing with calculations of the dispersion relation for monolayer graphene that is doped<sup>9,25-27</sup> as well as pristine graphene whose collective charge density oscillations are driven by temperature<sup>28</sup>. The work on gapped graphene<sup>10</sup> was partially motivated by the observation that when monolayer graphene is on a substrate such as boron nitride, an energy gap between the valence and conduction bands is produced yielding a plasmon and single-particle excitation spectrum which can be drastically different from gapless monolayer graphene. In Refs.<sup>9</sup> through<sup>10</sup>, a detailed calculation of the undamped plasmon excitations was carried out for all wavelengths. Although computationally challenging, these calculations proved useful since our goal is to obtain a full understanding of the response properties of nanoscale structures to external probes. In a recent paper<sup>29</sup>, it was demonstrated that the plasmon excitations in graphene has a linear dispersion rather than a square root dependence on the wave vector. This startling result came as a surprise because since theoretical calculations on free-standing graphene clearly does not yield a linear dependence in the long wavelength limit. As a matter of fact, this linear dependence of plasmon frequency on wave vector was initially attributed to local field corrections to the random-phase approximation. Horing<sup>30</sup> showed that when graphene is Coulomb-coupled to a conductor, the surface plasmon causes the low-frequency  $\pi$ -plasmon to have a linear dispersion. In this paper, we calculate the full dispersion relation for undamped plasmons in a hybrid monolayer graphene-conductor structure. We exploit our simulations to consider how the plasmon dispersion is affected when there is an energy gap between the valence and conduction bands, thereby generalizing the results in<sup>10</sup> where a surface is assumed to play a role.

The longitudinal excitation spectra of allowable modes will be determined from a knowledge of the frequency-dependent non-local dielectric function  $\epsilon(\mathbf{r}, \mathbf{r}'; \omega)$  of the composite system, which depends on the position coordinates  $\mathbf{r}$ ,  $\mathbf{r}'$  and frequency  $\omega$ . Alternatively, the normal modes correspond to the resonances of the inverse dielectric function  $K(\mathbf{r}, \mathbf{r}'; \omega)$  satisfying  $\int d\mathbf{r}'' K(\mathbf{r}, \mathbf{r}'; \omega)\epsilon(\mathbf{r}', \mathbf{r}''; \omega) = \delta(\mathbf{r} - \mathbf{r}'')$ . The significance of  $K(\mathbf{r}, \mathbf{r}'; \omega)$  is that it embodies many-body effects<sup>31,32</sup> through screening by the medium of an external potential  $U(\mathbf{r}'; \omega)$  to produce an effective potential  $V(\mathbf{r}; \omega) = \int d\mathbf{r}'' K(\mathbf{r}, \mathbf{r}''; \omega)U(\mathbf{r}''; \omega)$ . In Sec. II, we briefly review the formalism for calculating the inverse dielectric function for a 2D layer interacting with a semi-infinite conductor. Section III is devoted to our numerical results

for the dispersion relations at arbitrary wavelength for this hybrid structure. We show explicitly how the gap for monolayer graphene affects both the dispersion relation for the surface plasmon and the low-frequency acoustic mode. Specifically, we demonstrate that the low-frequency plasmon branch may exist in a region of frequency-wave vector space that was not obtained for free standing gapped graphene. We conclude with a summary of our results in Sec. IV.

## II. GENERAL FORMULATION OF THE PROBLEM

In this work, we consider a composite nano-scale system consisting of a 2D layer separated from a thick dielectric material. The 2D layer may be monolayer graphene (or a 2DEG such as a semiconductor inversion layer or HEMT (high electron mobility transistor)). The 2D graphene layer may have a gap, thereby broadening the applicability of the composite system model which also incorporates a separation layer and a semi-infinite plasma, as depicted in Fig. 1. The excitation spectra of allowable modes will be determined from a knowledge of the non-local dielectric function  $\epsilon(\mathbf{r}, \mathbf{r}'; \omega)$  which depends on position coordinates  $\mathbf{r}, \mathbf{r}'$  and frequency  $\omega$  or its inverse  $K(\mathbf{r}, \mathbf{r}'; \omega)$  satisfying  $\int d\mathbf{r}' K(\mathbf{r}, \mathbf{r}'; \omega) \epsilon(\mathbf{r}', \mathbf{r}''; \omega) = \delta(\mathbf{r}, \mathbf{r}'')$ . The self-consistent field structure for  $K(\mathbf{r}, \mathbf{r}'; \omega)$  is determined, using the technique of Ref. [30].

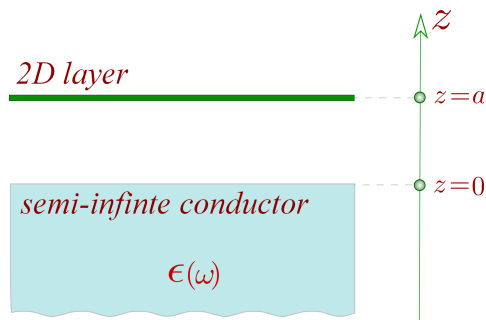


FIG. 1: (Color online) Schematic illustration of a thick (semi- infinite) metallic plasma interacting through the Coulomb force with a thin layer such as monolayer graphene.

In operator notation, the composite dielectric function  $\hat{\epsilon}$  and its inverse,  $\hat{K} = \hat{\epsilon}^{-1}$ , for the 2D layer and semi-infinite substrate is given by adding their polarizabilities  $\hat{\alpha}_{2D}$  and  $\hat{\alpha}_{SI}$ , respectively, i.e.,

$$\hat{K}^{-1} = \hat{\epsilon} = \hat{1} + \hat{\alpha}_{SI} + \hat{\alpha}_{2D} \equiv \hat{\epsilon}_{SI} + \hat{\alpha}_{2D} = \hat{K}_{SI}^{-1} + \hat{\alpha}_{2D} . \quad (1)$$

Multiplication of Eq. (1) from the right by  $\hat{K}$  and left by  $\hat{K}_{SI}$  yields the basic random-phase approximation (RPA) integral equation

$$\hat{K} = \hat{K}_{SI} - \hat{K}_{SI} \cdot \hat{\alpha}_{2D} \cdot \hat{K} . \quad (2)$$

Additionally,  $\hat{K}_{SI}$  is the inverse dielectric function for the semi-infinite substrate alone, whose surface lies in the  $z = 0$  plane. In explicit integral form, after Fourier transforming with respect to coordinates parallel to the translationally invariant  $xy$ -plane and suppressing the in-plane wave number  $q_{||}$  and frequency  $\omega$ , we obtain

$$K(z_1, z_2) = K_{SI}(z_1, z_2) - \int_{-\infty}^{\infty} dz' \int_{-\infty}^{\infty} dz'' K_{SI}(z_1, z') \alpha_{2D}(z', z'') K(z'', z_2) . \quad (3)$$

Here, the polarization function for the 2D layer is given by

$$\alpha_{2D}(z', z'') = \int_{-\infty}^{\infty} dz''' v(z', z''') D(z''', z'') , \quad (4)$$

where  $v$  is the Coulomb potential energy and the 2D response function's localization to the layer at  $z = a$  is expressed as

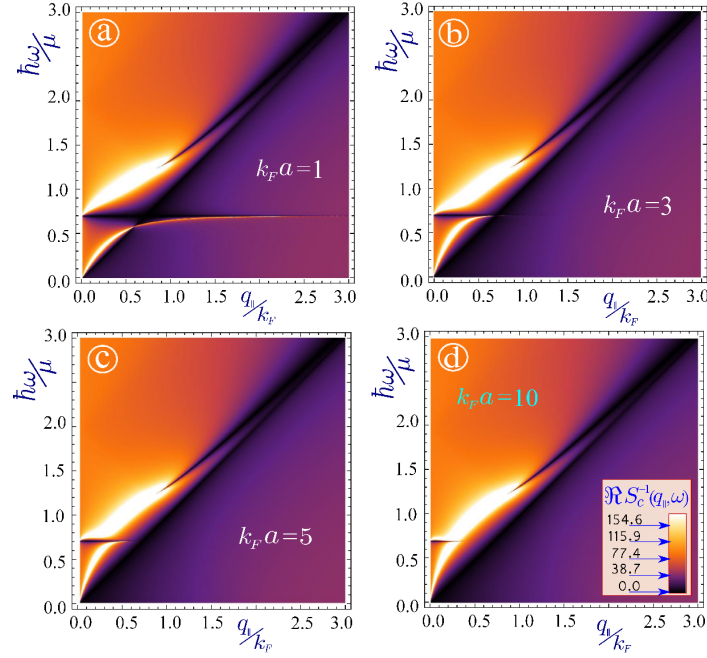


FIG. 2: (Color online) Density plots of the real part of the inverse of the dispersion function  $S_c(q_{\parallel}, \omega + i0^+)$  for extrinsic (doped) graphene with no band gap ( $\Delta = 0$ ) with the peaks corresponding to the plasmon resonances. Panels (a) – (d) demonstrate the plasmon spectrum for various separations between the graphene layer and the surface -  $a = 1, 3, 5$  and  $10 k_F^{-1}$ , where  $k_F$  is the Fermi wave number.

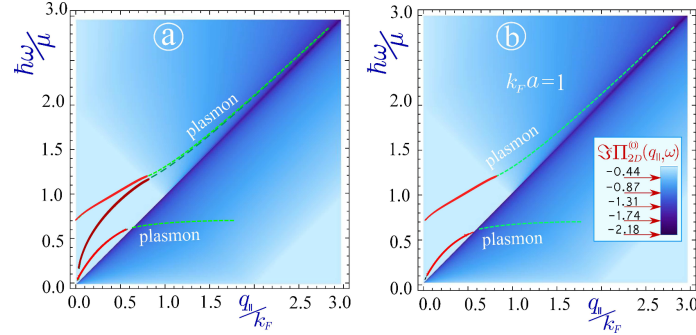


FIG. 3: (Color online) Exact numerical solutions for the plasmon dispersion of gapless graphene. In (a), the highest and lowest curves are the solutions of the plasmon dispersion equation  $\Re S_c(q_{\parallel}, \omega) = 0$  for graphene at a distance  $a = k_F^{-1}$  from a conducting surface, whereas the curve in between these two solutions corresponds to the zeros of  $1 + 2\pi e^2 / (\epsilon_s q_{\parallel}) \Re \Pi_{2D}^{(0)}(q_{\parallel}, \omega) = 0$  for free standing graphene. In (b), only the solutions for  $\Re S_c(q_{\parallel}, \omega) = 0$  are presented. In both (a) and (b), the plasmon energy is scaled with respect to the chemical potential  $\mu$  and we superimpose all plasmon curves on a background of a density plot of  $\Im \Pi_{2D}^{(0)}(q_{\parallel}, \omega)$  to illustrate the effects due to Landau damping.

$$D(z''', z'') = \Pi_{2D}^{(0)}(q_{\parallel}, \omega) \delta(z''' - a) \delta(z'' - a), \quad (5)$$

with  $\Pi_{2D}^{(0)}(q_{\parallel}, \omega)$  as the 2D ring diagram. Upon substituting this form of the polarization function for the monolayer into the integral equation for the composite inverse dielectric function  $K$ , we have

$$K(z_1, z_2) = K_{SI}(z_1, z_2) - \Pi_{2D}^{(0)}(q_{\parallel}, \omega) \int_{-\infty}^{\infty} dz' K_{SI}(z_1, z') v(z' - a) K(a, z_2). \quad (6)$$

We now set  $z_1 = a$  in Eq. (6) and obtain

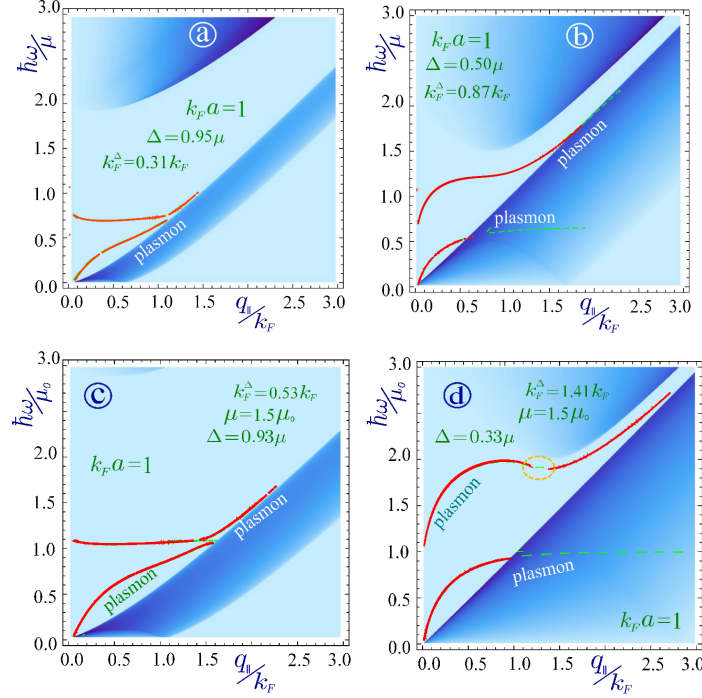


FIG. 4: (Color online) Exact numerical solutions of  $\Re S_C(q_{||}, \omega + i0^+) = 0$  for gapped graphene at a distance  $a = k_F^{-1}$  from a conducting surface. The plasmon excitation spectrum is superimposed on a background showing the density plot of  $\Im \Pi_{2D}^{(0)}(q_{||}, \omega + i0^+)$  whose values determine Landau damping. The red lines correspond to undamped plasmons when the magnitude of the plasmon dispersion function  $|S_C(q_{||}, \omega + i0^+)|$  vanishes. Panels (a) and (b) show the case of  $\Delta = 0.95\mu$  and  $0.5\mu$ , panels (c) and (d) demonstrate the behavior of the plasmon spectra for  $\mu = 1.5\mu_0$  and  $\Delta = 0.93\mu$  and  $\Delta = 0.33\mu$ , respectively. Here,  $\mu_0 = 0.2$  eV is the chemical potential used in the calculations of Fig. 3. This value for  $\mu_0$  is chosen to ensure the applicability of isotropy of the energy band structure at low doping.<sup>27</sup> Also, in our notation,  $k_F^\Delta \equiv \sqrt{\mu^2 - \Delta^2}/(\hbar v_F)$ .

$$K(a, z_2) = K_{SI}(a, z_2) - \Pi_{2D}^{(0)}(q_{||}, \omega) \left\{ \int_{-\infty}^{\infty} dz' K_{SI}(a, z') v(z' - a) \right\} K(a, z_2). \quad (7)$$

Solving algebraically for  $K(a, z_2)$  yields

$$K(a, z_2) = \frac{K_{SI}(a, z_2)}{S_C(q_{||}, \omega)} \quad (8)$$

with the “dispersion function”  $S_C(q_{||}, \omega)$  given by

$$S_C(q_{||}, \omega) \equiv 1 + \Pi_{2D}^{(0)}(q_{||}, \omega) \left\{ \int_{-\infty}^{\infty} dz' K_{SI}(a, z') v(z' - a) \right\}, \quad (9)$$

whose zeros determine the plasmon resonances of the composite system. In our numerical calculations, we employ  $K_{SI}(z, z')$  given by Eq. (30) of Ref. [32] for the semi-infinite metallic substrate in the local limit, whence Eqs. (6) through (9) yield<sup>30</sup>

$$K(z_1, z_2) = K_{SI}(z_1, z_2) - \Pi_{2D}^{(0)}(q_{||}, \omega) \frac{K_{SI}(a, z_2)}{S_C(q_{||}, \omega)} \left\{ \int_{-\infty}^{\infty} dz' K_{SI}(z_1, z') v(z' - a) \right\} \quad (10)$$

with



$$S_C(q_{||}, \omega) = 1 + \frac{2\pi e^2}{\epsilon_s q_{||}} \Pi_{2D}^{(0)}(q_{||}, \omega) \left\{ 1 + e^{-2aq_{||}} \frac{1 - \epsilon_B(\omega)}{1 + \epsilon_B(\omega)} \right\}. \quad (11)$$

Although the principal focus here is to examine the role of 2D graphene plasma nonlocality embedded in  $\Pi_{2D}^{(0)}(q_{||}, \omega)$  on the coupled plasmon spectrum of the composite system, we briefly revisit the local results of Ref.[30] to point out their generalization to include gapped graphene along with the previously discussed gapless results. In this regard, the graphene polarizability is also taken in the local limit with  $\Pi_{2D}^{(0)}(q_{||}, \omega) \approx Cq_{||}^2/\omega^2$  so that Eq. (11) yields

$$1 - \frac{2\pi C e^2}{\epsilon_s \omega^2} q_{||} \left\{ 1 + e^{-2aq_{||}} \frac{\omega_p^2}{2\omega^2 - \omega_p^2} \right\} = 0, \quad (12)$$

where the inclusion of a gap is described by

$$C = \frac{2\mu}{\pi \hbar^2} \left\{ 1 - \frac{\Delta^2}{\mu^2} \right\}, \quad (13)$$

$\mu$  is the chemical potential and  $\Delta$  is the gap between valence and conduction bands. Consequently, Eq. (12) yields the plasmon frequency as follows<sup>30</sup>:

$$\omega^2 = K_1 \pm \sqrt{K_2}, \quad (14)$$

with  $K_1$  and  $K_2$  defined by

$$\begin{aligned} K_1 &= \frac{\pi e^2 C}{\epsilon_s} q_{||} + \left( \frac{\omega_p}{2} \right)^2 \\ K_2 &= \frac{\pi e^2 C \omega_p^2}{\epsilon_s} e^{-2aq_{||}} q_{||} + \left[ \left( \frac{\omega_p}{2} \right)^2 - \frac{C e^2 \pi}{\epsilon} q_{||} \right]^2. \end{aligned} \quad (15)$$

In the low wave number limit  $q_{||} \ll 1/a$  these expressions are reduced to:

$$\begin{aligned} \omega_1 &\approx 2e \sqrt{\frac{\pi a C}{\epsilon_s}} q_{||} \\ \omega_2 &\approx \frac{\omega_p}{\sqrt{2}} + \frac{\sqrt{2} \pi C e^2}{\epsilon_s \omega_p} q_{||} \end{aligned} \quad (16)$$

which are both linear in  $q_{||}$ , differing from the  $q_{||}^{1/2}$ -dependence for free-standing graphene or the 2DEG<sup>9,10,33-36</sup>.

Nonlocality of the graphene plasma introduces changes in the features of  $K(z_1, z_2)$  of Eq. (10) and in its coupled 2D-surface plasmon spectrum in two respects. First, the local coupled mode spectrum described in the preceding paragraph is modified by nonlocality corrections in Eq. (11) with the use of the polarization function  $\Pi_{2D}^{(0)}(q_{||}, \omega)$  for all wave numbers as calculated by<sup>10</sup> for gapped graphene. Secondly, nonlocality introduces natural damping through the occurrence of regions in which plasmons can decay into electron-hole pairs consistent with energy-momentum conservation. The intersection of the plasmon dispersion curve  $\omega(q_{||})$  with such a particle-hole excitation region (PHER) signals the onset of damping at T=0K with  $\Im S_C(q_{||}, \omega) \neq 0$ . However, it is the undamped coupled plasmons that are of interest with

$$\Im S_C(q_{||}, \omega) = \Im \left( \Pi_{2D}^{(0)}(q_{||}, \omega) \right) \frac{2\pi e^2}{\epsilon_s q_{||}} \left\{ 1 + e^{-2aq_{||}} \frac{1 - \epsilon_B(\omega)}{1 + \epsilon_B(\omega)} \right\} = 0. \quad (17)$$

The features of the interacting graphene-surface plasmon spectrum are analyzed here numerically using the real and imaginary parts of the polarizabilities of Wunsch<sup>9</sup> for gapless graphene and Pyatkovskiy<sup>10</sup> for gapped graphene (all at zero temperature).

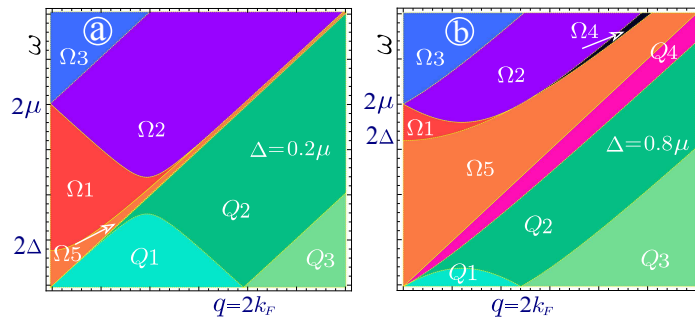


FIG. 5: (Color online) Schematics showing the regions having differing analytic expressions for the non-interaction polarization function  $\Pi_{2D}^{(0)}(q_{\parallel}, \omega)$ . Each part (real or imaginary) is determined by a different analytic expression, as in Refs. [10,13,14]. The regions with  $\omega > \hbar v_F q_{\parallel}$  are presented as  $\Omega 1 - \Omega 5$ , while the opposite are given by  $Q 1 - Q 4$ . Regions with non-zero  $\Im \Pi_{2D}^{(0)}(q_{\parallel}, \omega)$  are  $\Omega 1, \Omega 5, Q 4$  (where undamped plasmons exist) and  $Q 3$ . Plot (a) demonstrates the case of a small bandgap  $\Delta = 0.2\mu$ , whereas the panel (b) shows the case of relatively large gap  $\Delta = 0.6\mu$ .

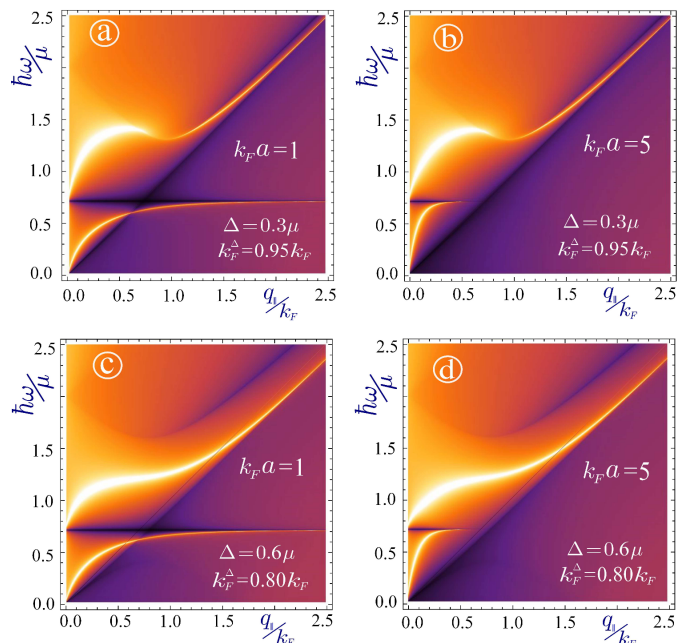


FIG. 6: (Color online) Density plot of the real part of the inverse dispersion function  $S_c(q_{\parallel}, \omega + i0^+)$  for extrinsic (doped) graphene having a finite band gap ( $\Delta \neq 0$ ) with the peaks corresponding to the plasmons. The panels are for various values of the energy gap  $\Delta$  and distance  $a$  between the surface and the graphene layer. Panel (a) shows the case when  $a = k_F^{-1}$  and  $\Delta = 0.3\mu$ , (b)  $a = 5k_F^{-1}$  and  $\Delta = 0.3\mu$ , (c)  $a = k_F^{-1}$  and  $\Delta = 0.6\mu$  and (d) describes  $a = 5k_F^{-1}$  and  $\Delta = 0.6\mu$ . We define  $k_F^{\Delta} \equiv \sqrt{\mu^2 - \Delta^2}/(\hbar v_F)$ .

### III. CALCULATED RESULTS AND DISCUSSION

First, we consider graphene with no energy gap and linear energy dispersion for the valence and conduction bands. The boundaries of the particle-hole modes region are linear, enclosing a triangular region, where the plasmons are not damped. The plasmons for gapless graphene are shown in Fig.[2]. We discern two plasmon branches, one attributed to the surface (the upper branch, originating from  $\omega_p/\sqrt{2}$  frequency) and the other to the graphene sheet (starting at the origin). We present results for various values of the distance  $a$  between the layer and the surface. When this separation is increased, the two branches evolve into a merged spectral line, similar to the plasmon of extrinsic gapless graphene. The surface plasmon branch tends to be dispersionless and to exist in the long wave length limit only. For all presented cases, the upper plasmon mode shows a stronger and broader peak. We display the absolute value of the real part of  $S_C^{-1}(q_{\parallel}, \omega)$  to emphasize each peak.

We also solve the equation  $\Re S_C(q_{\parallel}, \omega) = 0$  numerically, demonstrating the exact solution for the plasmon dispersion relation for both cases of zero (see Fig. 3) and finite (Fig. 4) energy band gap. These solutions become extremely interesting when the upper branch splits into two parts for the case of small energy gap. When the gap is zero, once again we see that the upper branch (which we attribute to the presence of a surface) adopts certain features of the plasmon in gapless graphene mainly because the branch is located in the same  $\{\omega, q_{\parallel}\}$  regions, both inside and outside the PHER. However, according to our analytical results, for long wavelengths both branches possess finite slope, in contrast to  $\propto \sqrt{q_{\parallel}}$  behavior in free standing graphene.

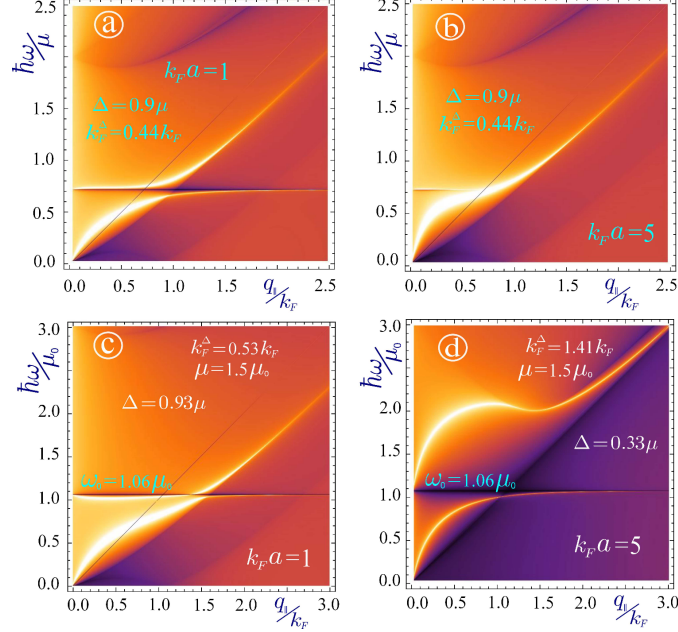


FIG. 7: (Color online) Density plot of the real part of the inverse dispersion function  $S_c(q_{\parallel}, \omega)$  for extrinsic (doped) graphene when the band gap is finite and where its peak positions correspond to the plasmon frequencies. The results in the panels were obtained for various chosen values of the energy gap  $\Delta$ , the distance  $a$  between the surface and the graphene layer and the chemical potential  $\mu$ , so that panel (a) shows the case when  $k_F a = 1$  and  $\Delta = 0.6\mu$ , (b)  $k_F a = 5$  and  $\Delta = 0.6\mu$ , (c)  $\mu = 1.5\mu_0$ ,  $k_F a = 1$  and  $\Delta = 0.93\mu$  and in (d)  $\mu = 1.5\mu_0$ ,  $k_F a = 1$  and  $\Delta = 0.33\mu$ . In our notation,  $\mu_0$  is an arbitrary doping, parameter in terms of which we measure chemical potential. We introduced  $k_F^\Delta \equiv \sqrt{\mu^2 - \Delta^2}/(\hbar v_F)$ .

The case of a small energy gap is presented in Fig. 4 for various energy gap and doping values. Similar to free standing graphene, the upper branch is extended due to splitting of the PHER. It might also be split into two different branches as mentioned in Ref. [10]. When the distance  $a$  of the 2D layer from the surface is increased, the two plasmon branches merge into a single branch, which is similar to the plasmon dispersion in gapped graphene. The general conclusion is that when one of the factors (energy gap, chemical potential or the separation  $a$ ) is appreciable, the changes caused by a sizable change in one of the others is not significant.

The role played by the energy band gap is an important part of our investigation. For monolayer graphene, an energy gap leads to an extended region of undamped plasmons<sup>10</sup>. In Fig. 5, we present the regions of the real and imaginary parts of the non-interacting polarization function which have distinct functional forms. We pay particular attention to the regions outside of the single-particle excitation continuum since, as mentioned previously, they encompass plasmon frequencies in the domains of  $\{\omega, q_{\parallel}\}$  where the plasmons are not damped. We denote these planar regions ( $\Omega_1$ ,  $\Omega_5$  and  $Q_4$ ) with reddish colors. The condition  $\Im \Pi_{2D}^{(0)}(q_{\parallel}, \omega) = 0$  is also satisfied in  $Q_3$ , but no plasmons are observed in this region. Region  $Q_4$  with  $\hbar v_F q_{\parallel} > \omega$  plays a crucial role in our study because this is where the extended undamped lower plasmon branch is located. This is a new situation, which was not encountered in previous works of Refs. [9,10,25,38] and it is attributed to screening by the carriers in the thick substrate adjoining the 2D layer.

Figure 7 exhibits our results for plasmon excitations of a composite system consisting of a layer of gapped graphene and a thick substrate for various values of the energy gap, chemical potential and the distance between the two bodies. The PHER and its boundaries constitute an important factor determining the plasmons. Consequently, the upper branch, located mainly in  $\Omega_1$  and  $\Omega_5$  regions, bears some similarity to the plasmons in free standing gapped

graphene, including its splitting into two parts in the vicinity of the boundary of  $\Omega_2$ . The results for both the lower and upper branches definitely depend on the gap. In the long wavelength limit, we demonstrate that  $\omega_1 \simeq \sqrt{C}$  and  $\omega_2 \simeq \omega_p/\sqrt{2} + \dots \simeq C$ , where  $C \simeq (1 - \Delta^2/\mu^2)$ . The plasmon dispersion relation for a free standing graphene layer with a finite energy gap is  $\omega \simeq \sqrt{Cq_{\parallel}}$ , which differs from our solution and Ref. [30]. However there is an interesting similarity in that the plasmon frequency is decreased with increased energy gap. This dependence is observed for increased values of  $q_{\parallel}$ .

The important differences in the plasmon spectra between free standing graphene and graphene interacting with a half space arise from the lower plasmon branch which lies on both sides of the straight line  $\omega = v_F q_{\parallel}$  and has a linear dispersion for small  $q_{\parallel}$ . According to previously published results<sup>10</sup>, the size of the  $Q4$  region is determined by doping as well as the energy gap. The boundary between  $Q4$  and  $Q2$  (with finite  $\Im\Pi_{2D}^{(0)}(q_{\parallel}, \omega)$ ) is described by  $\omega = -\mu + \sqrt{(\hbar v_F)^2(q_{\parallel} + k_F)^2 + \Delta^2}$  with  $\hbar v_F k_F = \sqrt{\mu^2 - \Delta^2}$ . For  $\Delta = 0$ , this boundary line is reduced to  $\omega = v_F q_{\parallel}$ . The plasmon dispersion for various doping concentrations is presented in Fig. 7. Increasing both  $\mu$  and  $\Delta$ , we find more extended branches where undamped plasmons exist. Figure 7(d) clearly demonstrates *anti-crossing* and an extended region of undamped plasmons for both branches. In all cases, the lower plasmon branch does not rise above the line  $\omega = \omega_p/\sqrt{2}$ . The curvature of the upper branch is determined by the ratio  $\Delta/\mu$  rather than by the gap itself. For certain values of this ratio, the upper branch consists of two different, separated plasmon branches.

We note that the exact numerical solutions in Fig. 4 corresponding to  $\Re S_C(q_{\parallel}, \omega) = 0$  are in agreement with the data for the density plots in Figs. 6 and 7. The results in these plots confirm the anti-crossing and the extension of the lower plasmon branches with increased doping and energy gap. We also note that for large values of the ratio  $\Delta/\mu \geq 0.9$  the lower branch becomes nearly dispersionless.

#### IV. CONCLUDING REMARKS

In summary, we have calculated the nonlocal plasmon dispersions within RPA for monolayer graphene interacting with a substrate, for arbitrary wavelength. In this, we investigated numerically the effects of the energy gap for extrinsic graphene, as well as the effects of its distance from the surface, on the plasmon dispersion relation. Our considerations were motivated by recent experimental work showing a linear plasmon dispersion in the long wavelength limit<sup>39</sup> and the subsequent theoretical work by one of the authors<sup>30</sup> to account for this observation, which is extended here to a fully general numerical description of nonlocal effects in monolayer graphene when the separation  $a$  is varied and when the energy gap is increased. Our new results in this paper vividly demonstrate that a thorough investigation necessitates incorporating the polarization into the dispersion equation at shorter wavelengths.

The distance  $a$  between monolayer graphene and the surface was varied in our nonlocal numerical calculations. In all cases, there are two plasmon branches; one originating from the surface plasmon and the other from the graphene layer. Both gapless and gapped graphene have been investigated. The most important consequence of introducing the energy gap in graphene is the extended region of undamped plasmons for both branches. Specifically, referring to Fig. 3(a), we note that the upper plasmon dispersion curve enters the gap in the particle-hole spectrum like that for gapped free standing graphene and these two curves are close to each other within this gap. In addition, the lower plasmon branch is undamped for a wider range of wave vectors  $q_{\parallel}$  by entering the gap in the particle-hole region. As revealed in Fig. 4(c), the lower branch may anti-cross with the upper one for sufficiently high doping concentration and large band gap. Both plasmon frequencies decrease with increased energy gap. This is also the behavior for free standing gapped graphene. However, the exact mathematical dependence is different in each case. Also, either one of the plasmon branches may bifurcate into two branches in the the single-particle excitation region, as demonstrated in Fig. 7(b). These new results for the plasmons may potentially lead to a number of applications in electronic devices since the plasmons play an important role in the response properties to external electromagnetic fields.

#### Acknowledgments

This research was supported by contract # FA 9453-13-1-0291 of AFRL. We thank Danhong Huang for helpful discussions.

---

<sup>1</sup> A. H. Castro Neto, F. Guinea, N. M. R. Peres, K. S. Novoselov, and A. K. Geim, Rev. Mod. Phys. **81**, 109 (2009)

<sup>2</sup> D. S. L. Abergela, V. Apalkov, J. Berashevicha, K. Ziegler, and Tapash Chakraborty, Adv. Phys. **59**, 261 (2010).

- <sup>3</sup> Luis E. F. Foa Torres, Stephan Roche and Jean-Christophe Charlier, Introduction to Graphene-Based Nanomaterials: From Electronic Structure to Quantum Transport”, Cambridge University Press. (2014).
- <sup>4</sup> G. Gumbs and D.H. Huang: Properties of Interacting Low-Dimensional Systems (Wiley-VCH Verlag GmbH & Co. KGaA, Boschstr, Weinheim, 2011).
- <sup>5</sup> D. H. Huang, Godfrey Gumbs, and Shawn-Yu Lin, Journ. Appl. Phys. **105**, 093715, (2009).
- <sup>6</sup> Godfrey Gumbs, Andrii Iurov, Antonios Balassis, and Danhong Huang, Journal of Physics: Condensed Matter, 26(13), 135601 (2014).
- <sup>7</sup> Andrii Iurov, Godfrey Gumbs, Bo Gao, and Danhong Huang, Applied Physics Letters, 104.20, 203103 (2014).
- <sup>8</sup> Antonios Balassis and Godfrey Gumbs, Phys. Rev. B 90, 075431 (2014).
- <sup>9</sup> B Wunsch, T Stauber, F Sols, and F Guinea, New Jour. of Phys. **8**, 318 (2006).
- <sup>10</sup> P. K. Pyatkovskiy, J. Phys.: Condens. Matter **21**, 025506 (2009).
- <sup>11</sup> Lin, M. F. and Shung, Kenneth W. -K., Phys. Rev. B, 50 , 23, 17744 (1994).
- <sup>12</sup> Wang, Y., Wang, X., Wu, Q., He, X. J., Gui, T. L., and Tong, Y. J., Plasmonics, 7(3), 411-415 (2012).
- <sup>13</sup> Cheng-Cheng Liu, Wanxiang Feng, and Yugui Yao, Phys.Rev.Lett. **107**, 076802 (2011).
- <sup>14</sup> C. J. Tabert and E. J. Nicol, Phys. Rev. B **89**, 195410 (2014).
- <sup>15</sup> Nordlander P, Oubre C, Prodan E, Li K and Stockman M I., Nano Lett., **4**, 5 (2004).
- <sup>16</sup> David J. Bergman and M. L. Stockman, Phys. Rev. Lett. **90**, 027402 (2003).
- <sup>17</sup> Tegenkamp, C., et al. ”Plasmon electronhole resonance in epitaxial graphene.” Journal of Physics: Condensed Matter 23.1 (2011): 012001.
- <sup>18</sup> Willets, Katherine A., and Richard P. Van Duyne. ”Localized surface plasmon resonance spectroscopy and sensing.” Annu. Rev. Phys. Chem. 58 (2007): 267-297.
- <sup>19</sup> Godfrey Gumbs, Andrii Iurov and Danhong Huang, arXiv:1410.2851 [cond-mat.mtrl-sci] (2014).
- <sup>20</sup> P. Sigmund: Particle Penetration and Radiation Effects (Springer- Verlag, Berlin, Heidelberg, 2006).
- <sup>21</sup> Pillai, S., et al. ”The effect of dielectric spacer thickness on surface plasmon enhanced solar cells for front and rear side depositions.” Journal of Applied Physics 109.7 (2011): 073105.
- <sup>22</sup> Goykhman, Ilya, et al., Nano letters 11.6 (2011): 2219-2224.
- <sup>23</sup> Bao, Wei, et al., Optics express 21.7 (2013): 8166-8176.
- <sup>24</sup> A. Satou, Y. Koseki, V. Ryzhii, V. Vyurkov, and T. Otsuji; arXiv:1401.3396 (2014).
- <sup>25</sup> K. W.-K. Shung, Phys. Rev. B **34**, 979 (1986).
- <sup>26</sup> Roslyak O, Gumbs G and Huang D 2011 J. Appl. Phys. 109 113721.
- <sup>27</sup> M Pizarra, A Sindona, P Riccardi, V M Silkin and J M Pitarke, New J. Phys. 16 083003 (2014).
- <sup>28</sup> S. Das Sarma and A. Madhukar, Phys. Rev. B **23**, 805 (1981).
- <sup>29</sup> C. Kramberger, R. Hambach, C. Giorgetti, M. H. Rmmeli, M. Knupfer, J. Fink, B. Bchner, L. Reining, E. Einarsson, S. Maruyama, F. Sottile, K. Hannewald, V. Olevano, A. G. Marinopoulos, and T. Pichler, Phys. Rev. Lett. **100**, 196803 (2008).
- <sup>30</sup> N. J. M. Horing, Phys. Rev. B **80**, 193401 (2009).
- <sup>31</sup> Kouzakov, Konstantin A., and Jamal Berakdar, Phys. Rev. A **85.2**, 022901 (2012).
- <sup>32</sup> N. J. M. Horing, Elliott Kamen, and Hong-Liang Cui, Phys. Rev. B **32**, 2184 (1985).
- <sup>33</sup> C. Steinebach, D. Heitmann, and V. Gudmundsson, Phys. Rev. B **56**, 6742 (1997).
- <sup>34</sup> B. P. van Zyl and E. Zaremba, Phys. Rev. B **59**, 2079 (1999).
- <sup>35</sup> S. A. Mikhailov, Phys. Rev. B **58**, 1517 (1998).
- <sup>36</sup> O. R. Matov, O. F. Meshkov, and, V. V. Popov, JETP **86**, 538 (1998).
- <sup>37</sup> R. Roldan, M.O. Goerbig and J.-N. Fuchs, Phys. Rev. B **80**, 085408 (2009)
- <sup>38</sup> S. Das Sarma and Q. Li, Phys. Rev. B **87**, 235418 (2014).
- <sup>39</sup> C. Kramberger, R. Hambach, C. Giorgetti, M. H. Rmmeli, M. Knupfer, J. Fink, B. Bchner, L. Reining, E. Einarsson, S. Maruyama, F. Sottile, K. Hannewald, V. Olevano, A. G. Marinopoulos, and T. Pichler, Phys. Rev. Lett. **100**, 196803 (2008).